



HAL
open science

Aqueous synthesis of highly luminescent ternary alloyed Mn-doped ZnSeS quantum dots capped with 2-mercaptopropionic acid

Salima Mabrouk, Hervé Rinnert, Lavinia Balan, Sébastien Blanchard, Jordane Jasniewski, Ghouti Medjahdi, Rafik Ben Chaabane, Raphaël Schneider

► To cite this version:

Salima Mabrouk, Hervé Rinnert, Lavinia Balan, Sébastien Blanchard, Jordane Jasniewski, et al.. Aqueous synthesis of highly luminescent ternary alloyed Mn-doped ZnSeS quantum dots capped with 2-mercaptopropionic acid. *Journal of Alloys and Compounds*, 2020, 858, pp.158315. 10.1016/j.jallcom.2020.158315 . hal-03087423

HAL Id: hal-03087423

<https://hal.univ-lorraine.fr/hal-03087423>

Submitted on 6 Jan 2021

HAL is a multi-disciplinary open access archive for the deposit and dissemination of scientific research documents, whether they are published or not. The documents may come from teaching and research institutions in France or abroad, or from public or private research centers.

L'archive ouverte pluridisciplinaire **HAL**, est destinée au dépôt et à la diffusion de documents scientifiques de niveau recherche, publiés ou non, émanant des établissements d'enseignement et de recherche français ou étrangers, des laboratoires publics ou privés.



Distributed under a Creative Commons Attribution - NonCommercial - NoDerivatives 4.0 International License

Aqueous synthesis of highly luminescent ternary alloyed Mn-doped ZnSeS quantum dots capped with 2-mercaptopropionic acid

Salima Mabrouk ^{a,b}, Hervé Rinnert ^c, Lavinia Balan ^d, Sébastien Blanchard ^e, Jordane Jasniewski ^f, Ghouti Medjahdi ^c, Rafik Ben Chaabane ^b, Raphaël Schneider ^{a,*}

^a Université de Lorraine, CNRS, LRGP, F-54000 Nancy, France

^b Laboratoire Interfaces et Matériaux Avancés, LIMA, LR011ES55, Faculté des Sciences de Monastir, Avenue de l'environnement, 5019, Tunisie

^c Université de Lorraine, CNRS, IJL, F-54000 Nancy, France

^d CEMHTI-UPR 3079 CNRS, Site Haute Température, 1D avenue de la Recherche Scientifique, 45071 Orléans, France

^e Sorbonne Université, CNRS, Institut Parisien de Chimie Moléculaire, IPCM, F-75005 Paris, France

^f Université de Lorraine, LIBio, F-54000 Nancy, France

* Corresponding author. E-mail address: raphael.schneider@univ-lorraine.fr

Abstract

Highly photoluminescent and water dispersible ternary alloyed Mn-doped ZnSeS and core/shell Mn:ZnSeS/ZnS quantum dots (QDs) with pure dopant emission were synthesized through a simple aqueous route using thiolactic acid (2-MPA) as a capping ligand. Transmission electron microscopy and X-ray diffraction show that Mn:ZnSeS nanocrystals are of spherical shape, with a diameter of 2.4 nm and a cubic zinc blende structure. With the overcoating of the ZnS shell, the particle size increases to 3.7 nm, which confirms the epitaxial growth of the shell on Mn:ZnSeS cores. The photoluminescence (PL) quantum yield depends on the Mn loading and reaches 22% for Mn:ZnSeS cores doped with 10% Mn and 41% after the growth of ZnS at the surface of the cores due to the effective elimination of surface-trap states. Mn:ZnSeS QDs exhibit also long PL lifetimes (up to 681 μ s) indicating that the emission originates from the spin forbidden $Mn^{2+} \ ^4T_1 \rightarrow \ ^6A_1$ transition. Electron paramagnetic resonance and X-ray photoelectron spectroscopy results suggest that Mn^{2+} ions

are located at the interface of core/shell Mn:ZnSeS/ZnS QDs. Further, the stability of Mn:ZnSeS/ZnS QDs was also investigated along with their transfer in organic phase using octanethiol.

Keywords: Quantum dots; Mn-doped ZnSeS; core/shell Mn:ZnSeS/ZnS; 2-mercaptopropionic acid; Photoluminescence; Stability

1. Introduction

In recent years, doped semiconductor nanocrystals (quantum dots, QDs) have attracted high interest due to the novel properties like optical, electronic or magnetic brought to QDs by the dopant [1-4]. Doping QDs with Mn^{2+} ions allows the engineering of nanocrystals with an emission usually located between 570 and 590 nm originating from the ${}^4T_1 \rightarrow {}^6A_1$ transition of Mn^{2+} ions in the host material [1-8]. Large bandgap QDs doped with Mn^{2+} exhibit a high Stokes shift that avoids self-absorption and the photoluminescence (PL) is of higher thermal stability than conventional binary or ternary semiconductor QDs which makes Mn-doped QDs of high potential for light-emitting diodes (LEDs) or laser applications [9]. Moreover, the PL lifetime of Mn-doped QDs is in the ms scale which allows to easily distinguish the dopant related emission from the background, which is of high interest for bio-applications [5,10,11]. Mn-doping is usually performed using wide bandgap semiconductors like ZnO, ZnS or ZnSe as host materials because the doping allows to tune their PL emission to the visible range but also due to the lower cytotoxicity of these QDs compared to Cd^{2+} -based ones. Mn-doped ZnS or ZnSe QDs can be prepared in organic or aqueous phase via the growth-doping or the nucleation-doping strategies, the latter being of high interest to uniformly dope the host nanocrystals [12-14]. High quality Mn:ZnS and Mn:ZnSe QDs with pure dopant emission and PL quantum yields (QYs) up to 50% are usually prepared at high temperature on organic medium using fatty acids or amines or tri-n-butylphosphine as capping agents [15-19].

Aqueous phase synthesis is an alternative method to produce Mn-doped ZnS or ZnSe QDs and affords dots dispersible in water without any ligand exchange or encapsulation. Moreover, the aqueous phase synthesis is cheaper and uses fewer toxic reagents than syntheses conducted in organic phase. However, the PL QYs of these QDs are lower than those prepared in organic media (values are usually below 24%) [20-23]. A dual emission of the dopant and of the host material is also sometimes observed. The PL QY of water

dispersible Mn:ZnS or Mn:ZnSe QDs can markedly be increased by introducing a ZnS shell at their surface [24]. When the shelling is conducted at high temperature under hydrothermal conditions or under microwave irradiation, S^{2-} ions diffuse from the shell into the ZnSe core to form ternary alloyed ZnSeS core QDs capped by a ZnS shell [25]. The formation of gradient alloyed ZnSe/ZnSeS with improved optical properties was also observed after the irradiation of thioacid-capped ZnSe QDs due to the light induced decomposition of the thiol-based ligand that generates S^{2-} ions [26]. Due to their high stability and enhanced PL QYs, ZnSeS and core/shell ZnSeS/ZnS QDs have been demonstrated to be of high potential for lasers, sensing and bioimaging [27-30].

Mn:ZnSeS and Mn:ZnSeS/ZnS QDs with PL QYs up to 50% and exhibiting pure dopant emission can be prepared at high temperature in organic media via the nucleation-doping strategy [31-33]. Only one recent report describes the hydrothermal synthesis of Mn:ZnSeS QDs with a dual dopant and defect related PL emissions and the PL QY of these nanocrystals was not provided [34].

We report here a new and easy aqueous synthesis of 2-MPA-capped Mn:ZnSeS and Mn:ZnSeS/ZnS QDs exhibiting PL QYs up to 41% for the core/shell nanocrystals, value that favourably compares with hydrophilic Mn:ZnSeS/ZnS QDs prepared in organic phase after their transfer to water. Moreover, Mn:ZnSeS and Mn:ZnSeS/ZnS QDs show almost pure dopant emission located at ca. 580 nm. Electron paramagnetic resonance (EPR) and X-ray photoelectron spectroscopy (XPS) results suggest that the dots were formed via a growth doping mechanism and that the Mn^{2+} dopant is localized at the interface between the core and the shell. Mn:ZnSeS and Mn:ZnSeS/ZnS QDs were also demonstrated to be of high stability under UV irradiation. Ligand exchanges can also be conducted on these nanocrystals without alteration of their optical properties.

2. Experimental section

2.1. Materials

Zinc nitrate hexahydrate $Zn(NO_3)_2 \cdot 6H_2O$ (> 99.0%, Sigma Aldrich), manganese acetate tetrahydrate $Mn(OAc)_2 \cdot 4H_2O$ (99%, ABCR), thiolactic acid, 2-MPA (95%, Sigma Aldrich), 3-mercaptopropionic acid, 3-MPA (> 99%, Sigma Aldrich), selenium powder (99.5+%, Sigma Aldrich), sodium borohydride (99%, Sigma Aldrich), sodium sulfide nonahydrate

(98.0% min, Alfa Aesar), 1-octanethiol (98%, Alfa Aesar), L-glutathione reduced GSH (> 98.0%, Sigma Aldrich), N-acetyl-L-cysteine NAC (> 99%, Sigma Aldrich) and 2-dimethylaminoethanethiol hydrochloride DMAT (95%, Acros Organics) were used without further purification.

2.2. Synthesis of Mn-doped ZnSeS cores

A one-pot three-steps method was developed for the preparation of Mn^{2+} -doped ZnSeS cores. The following synthetic protocol describes the preparation of the 10% Mn^{2+} -doped cores. In a three-necked flask, the metal precursors (0.75 mmol of $\text{Zn}(\text{NO}_3)_2$ and 0.075 mmol of $\text{Mn}(\text{OAc})_2$) and 2-MPA (100 μL , 1.147 mmol) are solubilized in 20 mL of ultrapure water at room temperature. The pH of the solution is adjusted to 7 by adding dropwise a 1 M NaOH aqueous solution and oxygen is removed from the reaction medium by bubbling with argon for 30 min. In another reaction flask, the NaHSe solution was prepared by reacting 0.215 mmol of Se(0) with 7.93 mmol of NaBH_4 in 4 mL of ultra-pure water. The solution becomes colorless after 10 min of stirring under argon. The NaHSe solution is then quickly injected into the reaction flask and stirring is maintained for 15 min. Next, $\text{Na}_2\text{S}\cdot 9\text{H}_2\text{O}$ (0.215 mmol) in 2 mL of water was quickly injected into the above mixture which is further stirred for 5 min at room temperature. Finally, the reaction mixture was heated at 100°C under argon. During the growth of Mn:ZnSeS QDs, aliquots were taken at various time intervals for UV-visible absorption and fluorescence analyses. After cooling to a room temperature, Mn:ZnSeS QDs were recovered by adding ethanol to the reaction mixture followed by centrifugation (1700 g for 15 min). Mn:ZnSeS QDs were purified by washing with ethanol (2 x 20 mL).

2.3. Overcoating Mn-doped ZnSeS cores with a ZnS shell

After a growth time of 7 h at 100°C , a ZnS shell was deposited at the surface of Mn-doped ZnSeS QDs. A monolayer of ZnS can be considered as a shell that measures 0.27 nm (the distance between consecutive planes in bulk cubic ZnS) along the major axis of the prolate-shaped dots [35]. Thus, one additional layer should increase the diameter by 0.54 nm. The amount of Zn^{2+} and S^{2-} precursors required for the introduction of one monolayer was determined by the number of surface atoms of a given size of Mn:ZnSeS/ZnS QDs. Considering that core ZnSeS QDs have an average diameter of ca. 2.4 nm (based on TEM experiments), one injection of $\text{Zn}(\text{NO}_3)_2$ and of $\text{Na}_2\text{S}\cdot 9\text{H}_2\text{O}/2\text{-MPA}$ stock solutions can be

considered to be a one monolayer addition. The ZnS shell cannot be assumed to coat the nanocrystals evenly to make up a perfect monolayer because the shape of the nanocrystals is not a perfect sphere.

To the Mn:ZnSeS crude cores at 100 °C were simultaneously added via two syringes 0.65 mL of a 0.15 M Zn(NO₃)₂ solution and 0.65 mL of a 0.1 M Na₂S·9H₂O/0.04 M 2-MPA solution (pH adjusted to 7). The same operation is repeated every hour. An injection of Zn²⁺ and S²⁻/2-MPA precursors is considered to allow the addition of a monolayer to the surface of Mn:ZnSeS cores. Aliquots were taken before each injection and the UV-visible absorption and fluorescence spectra were recorded to monitor the growth of the shell. When the reaction was completed, the core/shell Mn:ZnSeS/ZnS QDs were precipitated with ethanol, collected by centrifugation (1700 g for 15 min) and washed with ethanol (2 x 20 mL).

2.4. Photostability experiments

The photostability was evaluated by continuously irradiating an aqueous dispersion of Mn:ZnSeS/ZnS QDs with a Hg-Xe lamp for 1 h (light intensity of 50 mW/cm²). The optical properties were monitored by UV-visible and fluorescence spectroscopy.

2.5. Phase transfer

The phase transfer method reported by Tsay *et al.* [36] was used to transfer Mn:ZnSeS/ZnS QDs from an aqueous water to an organic medium, with slight modifications. To 2-MPA-capped Mn:ZnSeS/ZnS dispersed in water was added octanethiol (1 mL) and acetone (1.9 mL) used as interfacial solvent. The mixture was vigorously stirred and heated for 3 h at 60°C. A complete phase separation was observed. The organic layer containing octanethiol-capped Mn:ZnSeS/ZnS QDs was separated, diluted with toluene (4 mL) and further refluxed at 110°C for 4 h to repair the surface defects generated by the ligand exchange. Finally, after cooling to room temperature, QDs were precipitated with ethanol, recovered by centrifugation (1700 g for 15 min) and washed with ethanol (2 x 20 mL).

2.6. Characterization

Transmission electron microscopy (TEM) and high-resolution (HR-TEM) measurements were performed on a Philips CM200 instrument operating at 200 kV. A drop of the QDs dispersed

in water was deposited onto a carbon film-supported copper grid. The powder X-ray diffraction (XRD) patterns were recorded using a Panalytical X'Pert Pro MPD diffractometer using Cu K α radiation ($\lambda = 0.15418$ nm). The dried samples were placed on a silicon zero-background sample holder and the XRD patterns were recorded at room temperature. XRD patterns were analyzed using TOPAS (Bruker AXS, Version 4-2). Hydrodynamic QDs sizes, polydispersity indexes (PDI), and Zeta potential measurements were determined by dynamic light scattering (DLS) on a Zetasizer Nano ZS (green laser beam 532 nm) (Malvern Panalytical, UK), Cuvette DTS1070.

Thermogravimetric analysis (TGA) was conducted under air atmosphere from room temperature to 800°C at a heating rate of 10°C/min using a TGA/DSC1 STAR equipment (MettlerToledo). Inductively Coupled Plasma-Optical Emission Spectrometer (ICP-OES) measurements were conducted on a Varian 720-ES equipment.

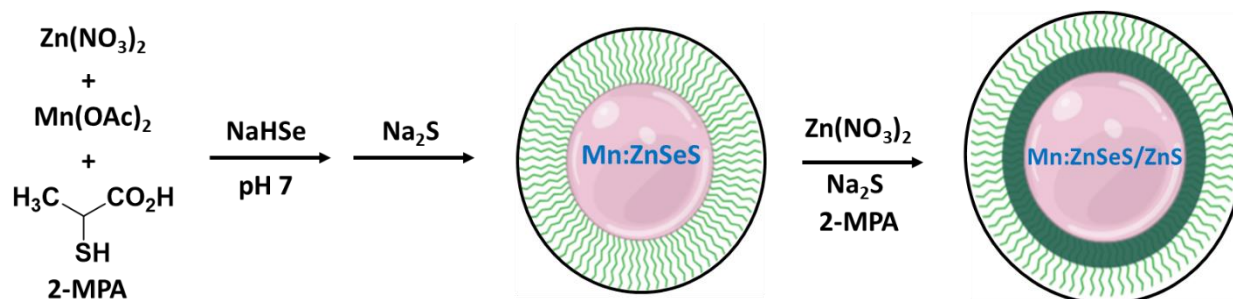
FT-IR absorption spectra were recorded on a Bruker ALPHA spectrometer. UV-visible absorption spectra were obtained with a Thermo Scientific Evolution 220 UV-visible spectrophotometer and photoluminescence (PL) emission spectra were recorded on a Horiba Fluoromax-4 Jobin Yvon spectrofluorometer. PL spectra were spectrally corrected and PL QYs were determined relative to Rhodamine 6G in ethanol (PL QY = 94%). For the time resolved photoluminescence (TR-PL) experiments, the QDs were pumped by the 355 nm line of a frequency-tripled YAG (yttrium aluminium garnet):Nd laser. The laser pulse frequency, energy and duration were typically equal to 10 Hz, 50 μ J and 10 ns, respectively. The PL signal was analysed by a monochromator equipped with a 600 grooves/mm grating and by a photomultiplier tube cooled at 190 K. The rise time of the detector is equal to around 3 ns.

X-band EPR spectra were recorded in non-saturating conditions on a Bruker ELEXSYS 500 spectrometer equipped with an Oxford instrument continuous-flow liquid-helium cryostat and a temperature control system. Typical conditions were : T = 20 K, 5 G amplitude modulation, $\nu = 9.402$ GHz and microwave power = 0.63 mW.

3. Results and discussion

3.1. Synthesis and optical properties of Mn-doped ZnSeS@2-MPA QDs

Mn-doped ZnSeS core QDs were prepared by reacting an aqueous solution of $\text{Zn}(\text{NO}_3)_2$, $\text{Mn}(\text{OAc})_2$ and the ligand with NaHSe and Na_2S at room temperature followed by heating at 100°C (Scheme 1).



Scheme 1. Schematic illustration for the aqueous-phase synthesis of Mn:ZnSeS QDs.

In preliminary experiments, we first evaluated the influence of the reactant ratio on the optical properties of Mn:ZnSeS QDs using 2-MPA as ligand and found that the highest PL intensity was obtained using a Zn/Se/S ratio of 1/0.28/0.28. The structure of the ligand was also varied. Experiments were conducted at $\text{pH } 7$ using 2-MPA, 3-mercaptopropionic acid (3-MPA), N-acetylcysteine (NAC) and glutathione (GSH) as capping ligands. As can be seen in Fig. S1, only the use of 2-MPA afforded Mn:ZnSeS QDs exhibiting almost pure dopant related emission at 582 nm. Using 3-MPA, NAC or GSH, a host surface defect-related emission located at 477 nm for 3-MPA and NAC and at 437 nm for GSH can be observed associated to the Mn^{2+} emission. These results suggest that the use of 3-MPA, NAC and GSH affords nanocrystals in which the energy transfer from the ZnSeS host to the Mn^{2+} dopant is not optimal. The signals at 477 and 437 nm are ascribed to Zn vacancies (V_{Zn}) and S or Se vacancies (V_{S} or V_{Se}), respectively [37,38]. Noteworthy is also the significant shift of the Mn^{2+} PL emission when varying the structure of the ligand (560, 581, 582 and 625 nm using NAC, 2-MPA, 3-MPA and GSH, respectively) which is related to the Mn^{2+} cations location in ZnSeS QDs or to Mn-Mn interactions [16,39].

Another important result observed in these preliminary tests is that undoped ZnSeS QDs prepared using 2-MPA as ligand exhibit almost no fluorescence (data not shown) while a strong defect state emission at 484 nm was observed when using 3-MPA (Fig. S2). Despite its structural similarities with 3-MPA, 2-MPA has very scarcely been used as ligand for the stabilization of QDs and no data are available related to its interactions with metal salts used to engineer the dots [40-42]. When adding the Mn^{2+} dopant in the reaction medium, almost pure dopant emission is observed after the injection of NaHSe and Na_2S , suggesting that 2-

MPA-capped MnSeS nuclei or related species are responsible for the PL emission observed. The FT-IR spectrum of pure 2-MPA shows signals at 2555 cm^{-1} (S-H stretching) and at 1699 cm^{-1} (C=O stretching) (Fig. S3). The SH signal disappears upon mixing with $\text{Zn}(\text{NO}_3)_2$ and $\text{Mn}(\text{OAc})_2$ and two signals characteristic of the asymmetric and of the symmetric stretching of carboxylate metal salts COOM (M = Zn or Mn) can be observed at 1563 and 1353 cm^{-1} , respectively [43]. As no PL is observed in the absence of Mn, we privilege the formation of bi- or polynuclear complexes like **2** and **3** rather than the monometallic complex **1** to be the species in solution before the addition of NaHSe and Na_2S (Fig. 1) [44,45]. The signals of the carboxylate function are markedly shifted to 1433 and 1329 cm^{-1} in Mn:ZnSeS and Mn:ZnSeS/ZnS QDs indicating that such metal-2-MPA complexes remain present at the surface of the dots after the growth step.

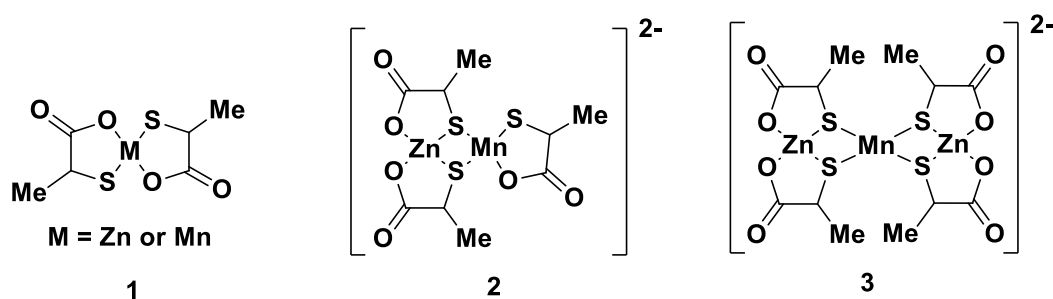


Fig. 1. Structures of the complexes formed between 2-MPA, $\text{Zn}(\text{NO}_3)_2$ and $\text{Mn}(\text{OAc})_2$.

Using 2-MPA as ligand, the influence of the pH of the reaction medium was also investigated. The highest PL intensity was observed at pH 7 and decreased significantly at pH 5 and especially at pH 9 (Fig. S4). The changes of pH during the synthesis had no influence on the crystallinity of Mn:ZnSeS QDs which exhibit a zinc blende structure (*vide infra*) (Fig. S5). The pH value of 7 was kept in all further experiments.

Fig. 2 shows the temporal evolution of UV-visible and the PL emission spectra of Mn:ZnSeS QDs (10% doping) during their growth at 100°C . The adsorption edge is located at ca. 380 nm. The first exciton absorption peak appearing as a shoulder shifts from 338 to 347 nm during the 7 h of heating, indicating the growth of the ZnSeS core (Fig. 2a). The ${}^4\text{T}_1 \rightarrow {}^6\text{A}_1$ emission of Mn^{2+} appears after 2 h of heating suggesting that both the formation rate of MnSeS nuclei and/or Mn-containing 2-MPA complexes and their incorporation into the ZnSeS host material are slow, which agrees well with results obtained for Mn:ZnSeS QDs prepared at high temperature in organic media [31]. A large Stokes shift of ca. 240 nm can be observed due to the high energy difference between the bandgap of the ZnSeS host and the $\text{Mn}^{2+} {}^4\text{T}_1 \rightarrow {}^6\text{A}_1$ d-d transition. The PL intensity increases gradually until 7 h, which confirms

the successful incorporation of Mn^{2+} in the ZnSeS host. Moreover, only a very weak defect related emission centered at ca. 480 nm can be observed for ZnSeS, indicating the efficient energy transfer between the ZnSeS host and the dopant. Extending the heating over 7 h caused a decrease of the PL intensity likely due to the increase of surface defects.

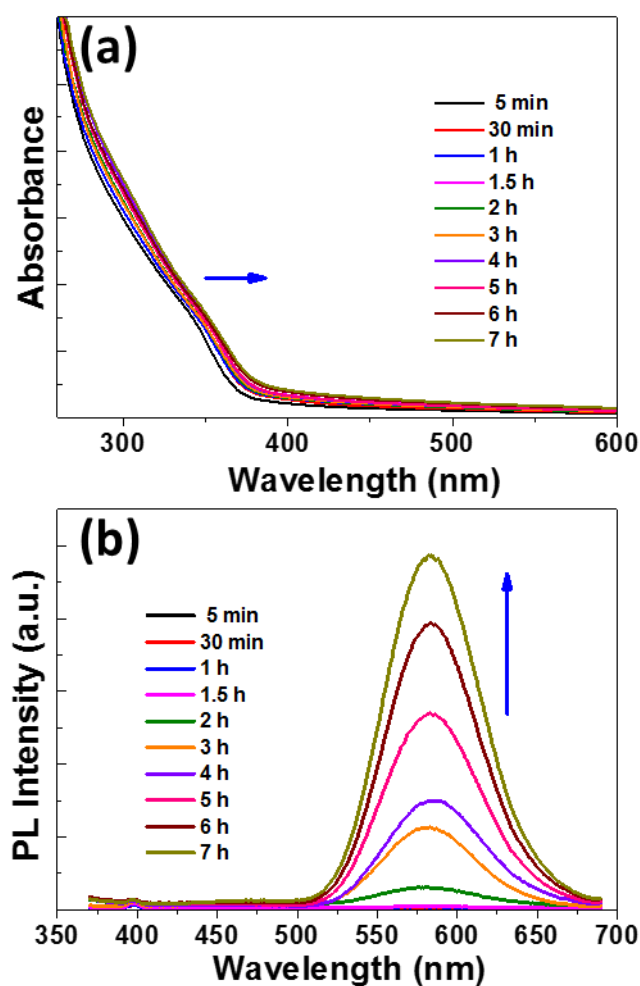


Fig. 2. Temporal evolution of (a) UV-visible and (b) PL emission spectra of Mn:ZnSeS QDs during the synthesis at 100°C.

Fig. 3a shows the PL emission spectra of Mn:ZnSeS QDs when varying the loading in Mn^{2+} (1.25, 2.5, 5, 10 and 15 mol% relative to Zn^{2+}). The PL intensity increases with the Mn^{2+} concentration and reaches its maximum for the 10% doping. A slight shift of the PL emission maximum from 574 to 580 nm is also observed with the increase of the Mn loading, which originates from Mn-Mn interactions in Mn:ZnSeS nanocrystals [5]. Simultaneously, the PL QY increases with the loading in Mn (values of 5.1, 6.3, 17.7 and 22% were measured for the

doping percentages of 1.25, 2.5, 5 and 10%, respectively). Further increasing the Mn^{2+} concentration was found to be deleterious on the PL QY (15.1% for the sample doped with 15% Mn) likely due to a self-quenching caused by the proximity of Mn^{2+} emission centers in the QDs [5]. No defects were generated in the ZnSeS crystal lattice by the Mn^{2+} loading as demonstrated by XRD (*vide infra*). Noteworthy is also that the amount of Mn^{2+} incorporated in ZnSeS QDs is markedly lower than the nominal Mn^{2+} value as observed by XPS analysis (*vide infra*). The actual doping percentages are of 0.31, 0.57, 1.33 and 1.66% for initial loading of 1.25, 2.5, 5 and 10% Mn^{2+} . The amounts of Zn and Mn elements were also quantified using ICP-OES. Mn/Zn ratios of 0.29/100, 0.51/100, 1.40/100 and 1.65/100 were determined for feed ratios of 1.25/100, 2.5/100, 5/100 and 10/100, respectively. These results are in good agreement with XPS analyses and confirm the low reactivity of 2-MPA-capped MnSeS nuclei or 2-MPA-Mn complexes that only weakly incorporate into the ZnSeS host material.

Time-resolved PL decay measurements were conducted to understand the PL emission mechanism. The PL decays were recorded at the PL maximum of Mn:ZnSeS QDs when varying the dopant concentration from 1.25 to 10% and are shown in Fig. 3b. The data were best fitted to a bi-exponential function $I(t) = A_1 \exp(-t/\tau_1) + A_2 \exp(-t/\tau_2)$, where τ_1 and τ_2 are the time constants of the PL and A_1 and A_2 the normalized amplitudes of the components. The average lifetime τ_{av} was determined using the formula $\tau_{av} = (A_1\tau_1 + A_2\tau_2)/(A_1 + A_2)$. The time constants are given in Table 1. The PL decays are characterized by a short lifetime τ_1 varying from 14 to 122 ns and a long lifetime τ_2 varying from 700 μs to ca. 1 ms with the increase of the Mn^{2+} doping. The fast lifetime corresponds to the defect state emission eventually combined with a non-radiative decay and the slow one to the spin forbidden $\text{Mn}^{2+} {}^4\text{T}_1 \rightarrow {}^6\text{A}_1$ transition of the electrons in the ZnSeS host [7,19]. The A_2 contribution is significantly higher for the 5 and 10% doping in Mn, which agrees well with the PL QYs determined for the dots. Finally, the average lifetime τ_{av} are of ca. 85 μs for 1.25 and 2.5 doping in Mn^{2+} but markedly increase for the 5 and 10% doping to 295 and 681 μs , which agrees well with values reported in the literature for Mn-doped ZnSeS [33] and Mn-doped ZnS or ZnSe QDs [16].

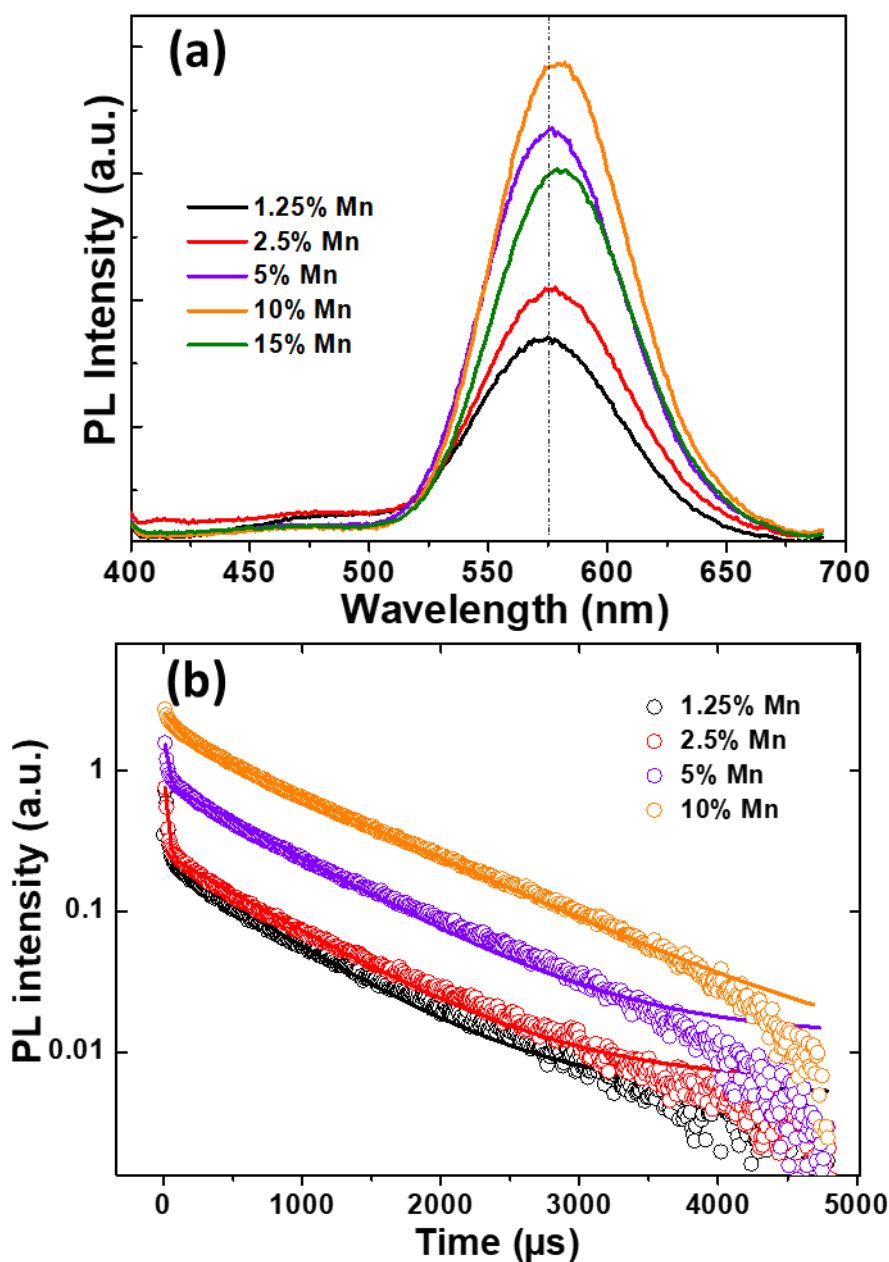


Fig. 3. (a) PL emission spectra of Mn:ZnSeS QDs when varying the Mn^{2+} dopant percentage (reactions were conducted at pH 7 and the heating time was fixed at 7 h), (b) PL decay curves of Mn:ZnSeS QDs when varying the Mn^{2+} loading. Spectra were recorded at the maximum emission wavelength and an excitation of 355 nm was used.

Table 1. Time constant τ_1 and τ_2 and the contributions of decays A_1 and A_2 of Mn:ZnSeS QDs when varying the dopant percentage from 1.25 to 10%.

| Sample | A_1 | τ_1 (ns) | A_2 | τ_2 (μs) | τ_{av} (μs) |
|--------|-------|------------------|-------|-------------------------------|----------------------------------|
|--------|-------|------------------|-------|-------------------------------|----------------------------------|

| | | | | | |
|----------------|--------|------|--------|-----|---------|
| Mn(1.25):ZnSeS | 0.0148 | 14.1 | 0.0021 | 701 | 87.113 |
| Mn(2.5):ZnSeS | 0.0197 | 17.7 | 0.0025 | 758 | 85.376 |
| Mn(5):ZnSeS | 0.0133 | 21.4 | 0.0081 | 781 | 295.625 |
| Mn(10):ZnSeS | 0.0077 | 122 | 0.0181 | 972 | 681.943 |

3.2. Optical properties of core/shell Mn:ZnSeS/ZnS QDs

The epitaxial growth of a ZnS shell at the surface of the Mn(10):ZnSeS QDs was conducted by simultaneously injecting $\text{Zn}(\text{NO}_3)_2$ and $\text{Na}_2\text{S}/2\text{-MPA}$ aqueous solutions each hour into the reaction mixture at 100°C after 7 h of core growth (Scheme 1). Each injection corresponds to a monolayer of ZnS grown at the periphery of Mn:ZnSeS QDs. ZnS is a wide bandgap semiconductor ($E_{\text{g,bulk}} = 3.7$ eV) and core/shell Mn:ZnSeS/ZnS QDs will be of type-I [24]. The ZnS shell should not only constitute a barrier protecting the optically active Mn:ZnSeS core from the surrounding aqueous medium but also passivate surface trap states and thus improve the PL QY [24]. During the shell growth, a redshift of both UV-visible absorption (from 360 to 367 nm) and of PL emission spectra (from 582 to 586 nm) was observed, which clearly indicates the deposition of the ZnS shell without any diffusion of S^{2-} or substitution of Mn^{2+} by Zn^{2+} into the ZnSeS core (Fig. 4a-b). These anion and cation exchanges would result in a blue shift of the UV-visible absorption spectra and to a decrease of the Mn^{2+} related emission, respectively. An increase of the PL intensity was observed until five monolayers of ZnS were added at the surface of Mn:ZnSeS. A marked increase of the PL QY from 22% to 41% was also observed after the shell growth due to the promotion of radiative recombination pathways. Further increasing the thickness of the ZnS shell caused a decrease of the PL QY likely due to the weak lattice contraction observed after introduction of the ZnS shell at the surface of the ZnSeS core (a values of 0.551 and 0.542 nm were determined for Mn:ZnSeS and Mn:ZnSeS/ZnS QDs, respectively, see Fig. S6 and Fig. S7.)

The PL decay curves of Mn:ZnSeS and Mn:ZnSeS/ZnS QDs are presented in Fig. 3c and, as previously, were fitted by a biexponential function. The PL lifetime parameters are summarized in Table 2. A slight decrease of the long PL lifetime τ_2 is observed after introduction of the ZnS shell from 972 μs for Mn:ZnSeS QDs to 792 μs for Mn:ZnSeS/ZnS QDs. As the PL QY of core/shell QDs is significantly enhanced and as surface defects and traps are expected to be removed, the decrease of the PL lifetime may arise from a modification of the Mn^{2+} local environment due to the introduction of the ZnS shell. In

addition, a partial diffusion of Mn^{2+} ions from the ZnSeS core to the ZnS shell cannot be excluded.

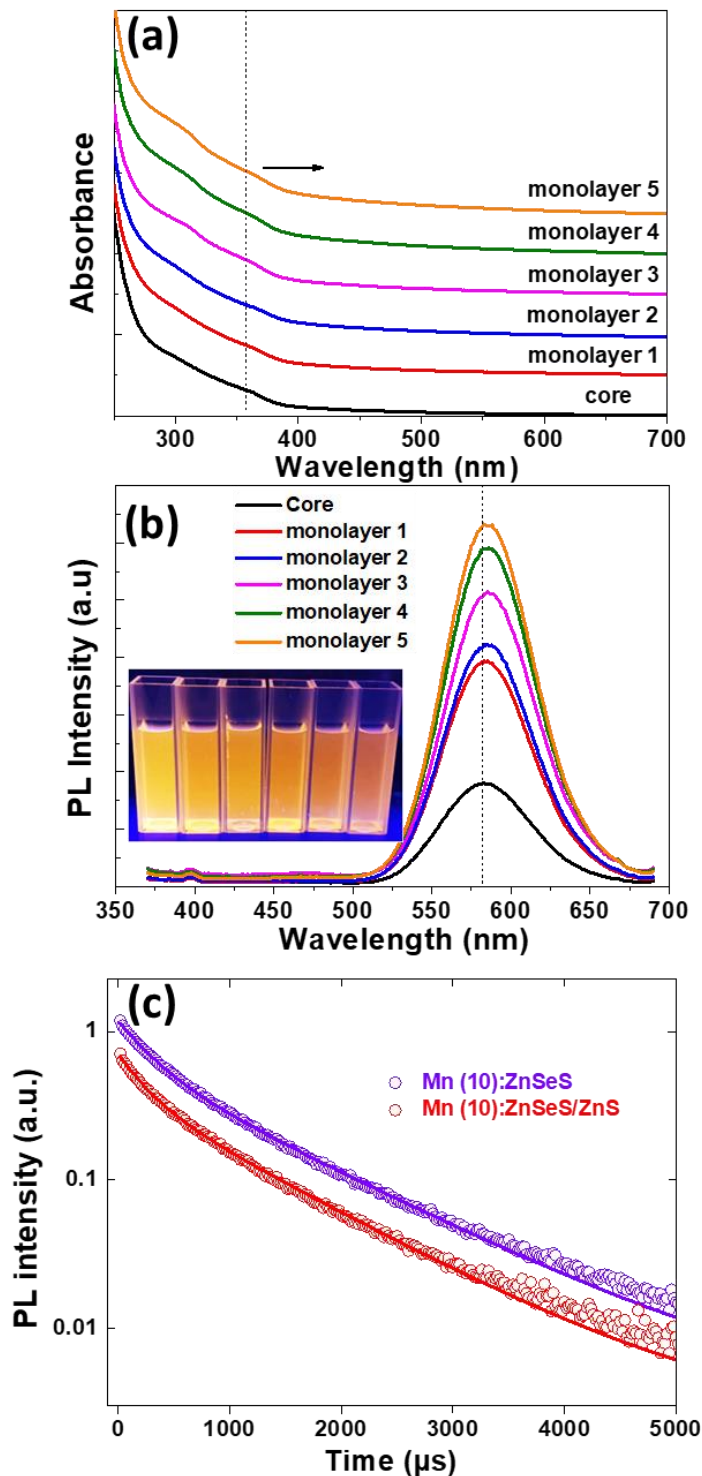


Fig. 4. Temporal evolution of (a) UV-visible and (b) PL emission spectra of Mn(10):ZnSeS QDs during the shell growth and (c) PL decay curves of Mn(10):ZnSeS and Mn(10):ZnSeS/ZnS QDs. Spectra were recorded at the maximum emission wavelength and an

excitation wavelength of 355 nm was used. The inset of (b) is a digital picture taken under UV light illumination of Mn(10):ZnSeS QDs during the deposition of the ZnS shell.

Table 2. Time constants τ_1 and τ_2 and the contributions of decays A_1 and A_2 of the 10% Mn-doped ZnSeS cores and the 10% Mn-doped ZnSeS/ZnS core/shell QDs.

| Sample | A_1 | τ_1 (ns) | A_2 | τ_2 (μ s) | τ_{av} (μ s) |
|------------------|--------|------------------|--------|------------------------|---------------------------|
| Mn(10)ZnSeS | 0.0077 | 122 | 0.0181 | 972 | 681.943 |
| Mn(10)/ZnSeS/ZnS | 0.0047 | 111.6 | 0.0102 | 792 | 542.209 |

3.3. Structural properties of Mn:ZnSeS and core/shell Mn:ZnSeS/ZnS QDs

Electron paramagnetic resonance (EPR) was further used to investigate the local environment around the Mn^{2+} dopant in Mn:ZnSeS QDs (Fig. 5). The six-line hyperfine structure originating from the interaction between the electronic spin and the ^{55}Mn nuclear spin ($I = 5/2$) can only clearly be observed for ZnSeS QDs doped with 1.25% Mn. The A value is high (ca. 88 G) indicating that Mn^{2+} ions are most likely in an octahedral environment, and thus located near the surface of ZnSeS QDs, which agrees well with the presence of Mn-2-MPA complexes observed by FT-IR [16]. Much lower values of A were measured for Mn^{2+} ions substituting Zn^{2+} ions at the tetrahedral sites in ZnS or ZnSe nanocrystals (68.4 and 66.1 G, respectively) [12,16,46,47]. Moreover, while in the latter case sharp peaks are observed, a significant line broadening is observed for all our EPR spectra. This line broadening very likely results from significant g-strain due to slight variations of the Mn-2-MPA complex environment at the surface of the QDs, again as opposed to Mn^{2+} substitution in tetrahedral site where no g-strain (sharp peaks) is observed. Additionally, the more pronounced line broadening observed for higher loading very likely originates from Mn-Mn interactions, suggesting increasing proximity between the Mn^{2+} ions at the surface of ZnSeS QDs. The signal of Mn^{2+} is still present after the ZnS shell growth, indicating that Mn^{2+} ions do not diffuse out of the ZnSeS/ZnS nanocrystals.

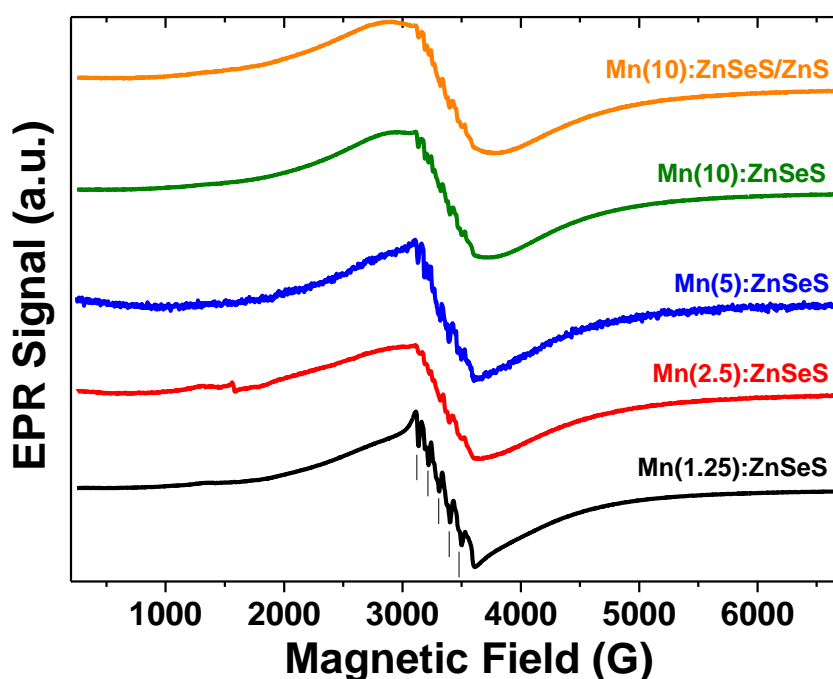


Fig. 5. EPR spectra recorded at 20 K of ZnSeS QDs loaded with 1.25, 2.5, 5 or 10% Mn^{2+} and of core/shell Mn(10)ZnSeS/ZnS QDs.

Fig. 6 shows the powder XRD patterns of Mn:ZnSeS QDs when varying the Mn^{2+} loading from 1.25 to 10% and of the core/shell Mn(10)ZnSeS/ZnS QDs. The peaks located at 28.2, 46.8 and 55.5° can be attributed to the (111), (220) and (311) planes of the cubic zinc blende phase of the ZnSeS host material and their broadness is indicative of the small size of the nanocrystals. The diffraction peaks are located between those of cubic ZnSe (JCPDS No 03-065-9603) and of cubic ZnS (JCPDS No 04-004-2829), which confirms the formation of the ternary alloyed ZnSeS host (the standard XRD patterns of bulk zinc blende ZnS and ZnSe are shown at the bottom of Fig. 6). No significant changes in XRD patterns were observed when increasing the Mn^{2+} dopant percentage, indicating that the ZnSeS crystal lattice is well preserved after the doping and that their compositions are similar. The XRD pattern of Mn:ZnSeS and Mn:ZnSeS/ZnS QDs fits well with that of the host with a $\text{ZnSe}_{0.5}\text{S}_{0.5}$ composition (Fig. S6 and S7 for the experimental and calculated data) indicating that both Se^{2-} and S^{2-} incorporate similarly in the crystal lattice. After introduction of the ZnS shell, the diffraction peaks further shift to the cubic ZnS phase, which is consistent with previous reports [27,31].

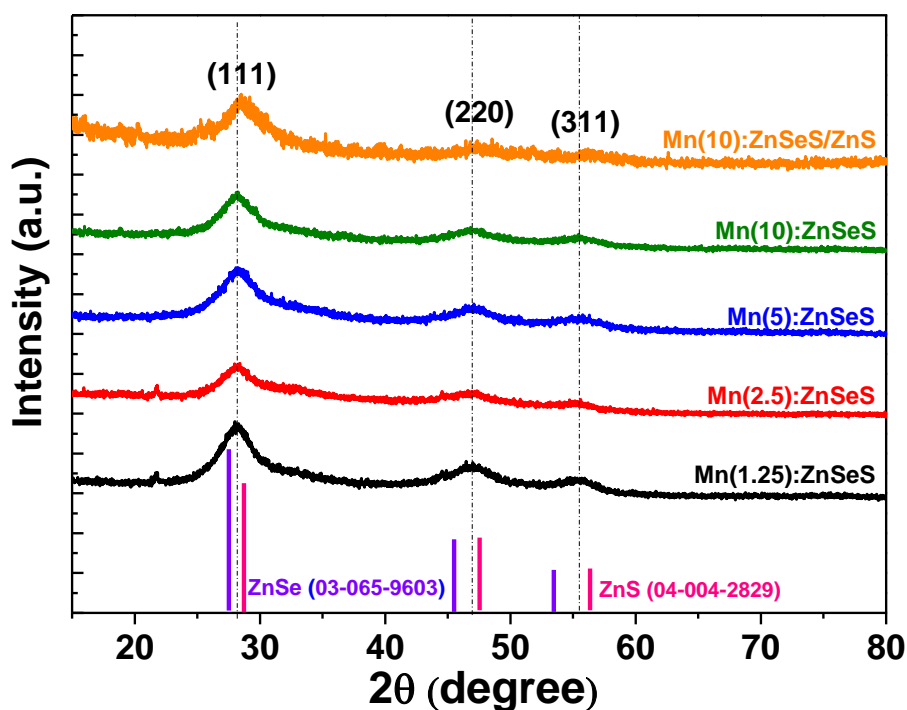


Fig. 6. XRD patterns of Mn:ZnSeS QDs when varying the Mn^{2+} dopant percentage and of core/shell Mn(10):ZnSeS/ZnS QDs.

TEM and HR-TEM measurements were conducted to determine the size and the structure of Mn(10):ZnSeS and Mn(10):ZnSeS/ZnS QDs. For both samples, particles with a nearly spherical shape and a well crystalline structure can be observed. The average diameter of Mn(10):ZnSeS QDs was determined to be $2.4 \text{ nm} \pm 0.8 \text{ nm}$ (Fig. 7a). After ZnS shelling, the average particles diameter increases to $3.7 \text{ nm} \pm 0.9 \text{ nm}$ (Fig. 7b). Mn(10):ZnSeS/ZnS core/shell QDs retain the nearly monodisperse size distribution of the Mn(10):ZnSeS cores, which indicates the successful epitaxial growth of the ZnS shell on Mn(10):ZnSeS cores. Considering a thickness of 0.27 nm for a monolayer of ZnS, the thickness of the ZnS shell at the periphery of Mn:ZnSeS QDs is estimated to be of ca. 2.4 monolayers, value lower than the theoretical number of monolayers deposited at the surface of the cores. Well-resolved lattice fringes indicate the crystalline structure of both QDs. The interplanar distance measured for the Mn:ZnSeS and Mn:ZnSeS/ZnS QDs is of 0.31 nm (Fig. 7c,e), value close to the (111) plane of zinc blende ZnSe (0.327 nm) and ZnS (0.312 nm) [29]. The cubic structure of the dots was further confirmed by the selected area electron diffraction patterns (Fig. 7d,f). It should also be noted that no obvious crystal interface could be observed in Mn:ZnSeS/ZnS QDs due to the close lattice constants of ZnSeS and ZnS.

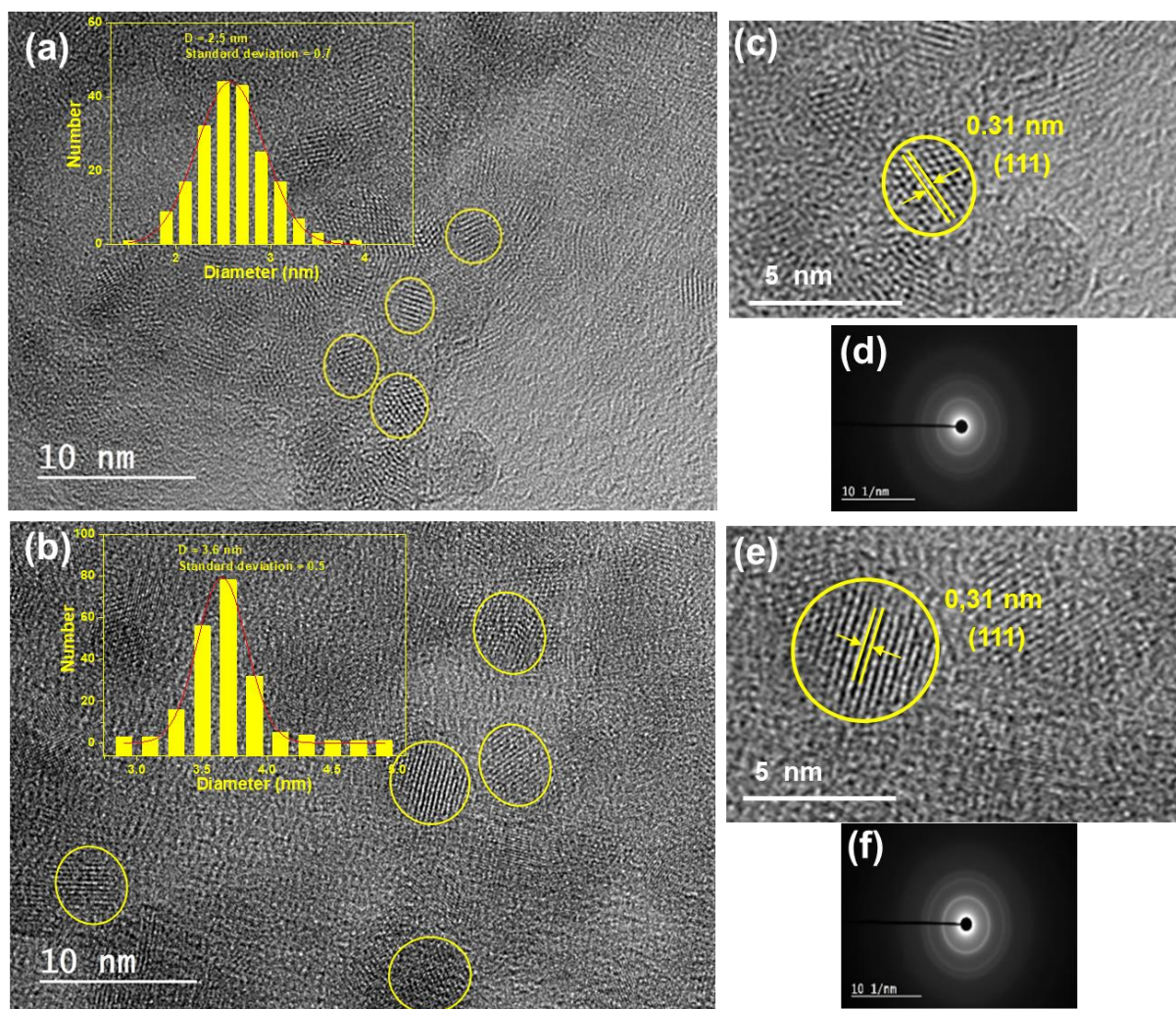


Fig. 7. TEM and HR-TEM images of (a,c) core Mn(10):ZnSeS and of (b,e) core/shell Mn(10):ZnSeS/ZnS QDs. The insets of (a) and (b) are the size distribution histograms and (d,f) are the SAED patterns.

X-ray photoelectron spectroscopy (XPS) measurements were further conducted to investigate the chemical state as well as the elemental composition of Mn:ZnSeS and of Mn:ZnSeS/ZnS QDs (Fig. S8 and S9, respectively). As shown in the overview spectrum of the Mn(10):ZnSeS QDs selected as a representative, only Zn, Se, S and Mn elements which compose the core of the nanocrystals as well as O and C elements present in the 2-MPA ligand can be detected (Fig. S8). The Zn $2p_{3/2}$ signal is located at 1021.42 eV, which corresponds to Zn^{+2} . The broad signal observed for Se originates from the overlap of Se $3d_{5/2}$ (53.49 eV) and Se $3d_{3/2}$ (54.35 eV) peaks. The energy splitting of 0.86 eV confirms that Se is in the -2 chemical state and bound to Zn [19,32,48]. The signal of S can be deconvoluted into four components, 161.40

and 162.60 eV for S 2p_{3/2} and S 2p_{1/2} in the lattice, respectively, and 163.70 and 164.90 eV for S 2p_{3/2} and S 2p_{1/2} of the 2-MPA ligand, respectively [32]. The separation between S 2p_{3/2} and S 2p_{1/2} peaks is of 1.2 eV, indicating that S is present in the -2 state. Finally, the Mn 2p_{3/2} signal is of low intensity and located at 639.06 eV. XPS overview and HR spectra of core/shell Mn(10):ZnSeS/ZnS@2-MPA QDs are shown in Fig. S9 and no marked changes in the binding energies were observed for Zn, Se, and S compared to the native Mn(10):ZnSeS core. The decrease of the Se/Zn atomic ratio (from 0.37 to 0.24) and the increase of the S/Zn atomic ratio (from 0.83 to 1.37) further confirm the successful growth of the ZnS shell at the surface of ZnSeS core. A significant shift to a higher binding energy was observed for Mn 2p_{3/2} (from 639.06 to 641.25 eV), indicating that Mn²⁺ ions are likely located at the interface between the ZnSeS core and the ZnS shell and bound to S rather than to Se (Fig. 8) [49].

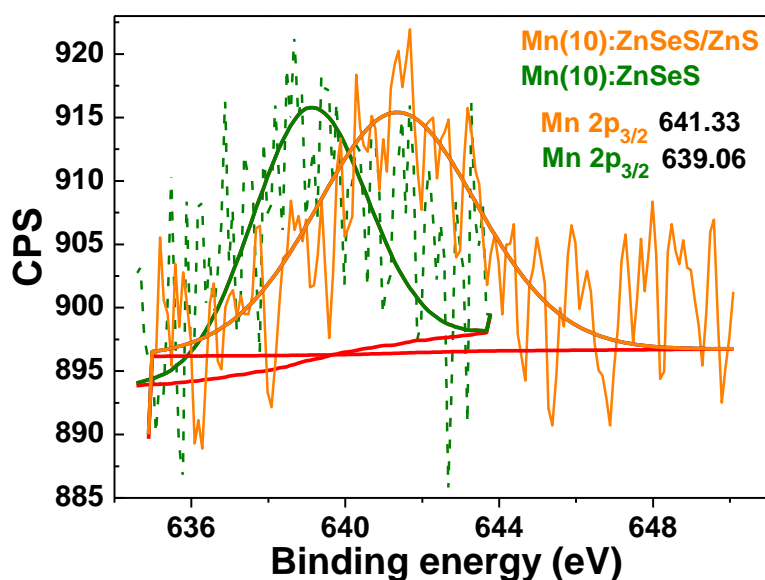


Fig. 8. High-resolution XPS spectra of Mn 2p for Mn(10):ZnSeS and Mn(10):ZnSeS/ZnS QDs.

3.4. Stability of Mn:ZnSeS/ZnS QDs

The influence of the pH on the PL intensity of a colloidal dispersion of Mn(10):ZnSeS/ZnS@2-MPA QDs was first evaluated (Fig. 9a). Aqueous 0.1 M solutions of NaOH or HCl were used to adjust the pH of the starting neutral dispersion. The PL intensity of Mn:ZnSeS/ZnS@2-MPA QDs increased gradually with the pH and reached its maximum at pH 11-12. A progressive decline of the PL intensity is observed until pH 5 followed by a

fast drop due the protonation of the carboxylate function of 2-MPA ($pK_a = 4.35$). QDs precipitate below pH 4 and the fluorescence disappears.

The photostability of Mn(10):ZnSeS@2-MPA and Mn(10):ZnSeS/ZnS@2-MPA QDs was also investigated under the continuous irradiation of Hg-Xe light (intensity of 50 mW/cm^2) under open air condition and at room temperature (Fig. 9b). A continuous increase of the PL intensity was observed for both QDs during the irradiation likely due to the partial decomposition of Zn^{2+} -2-MPA complexes adsorbed at the surface of the QDs and/or of the 2-MPA ligand into S^{2-} ions followed by the deposition of an extra ZnS shell at the surface of the dots (see Fig. S10 and S11 for the UV-visible absorption and PL emission spectra obtained with Mn:ZnSeS@2-MPA and Mn:ZnSeS/ZnS@2-MPA QDs, respectively). These results show that the ZnS shell introduced after synthesis as well as that formed during irradiation improves the dopant emission and protects the QDs from photobleaching

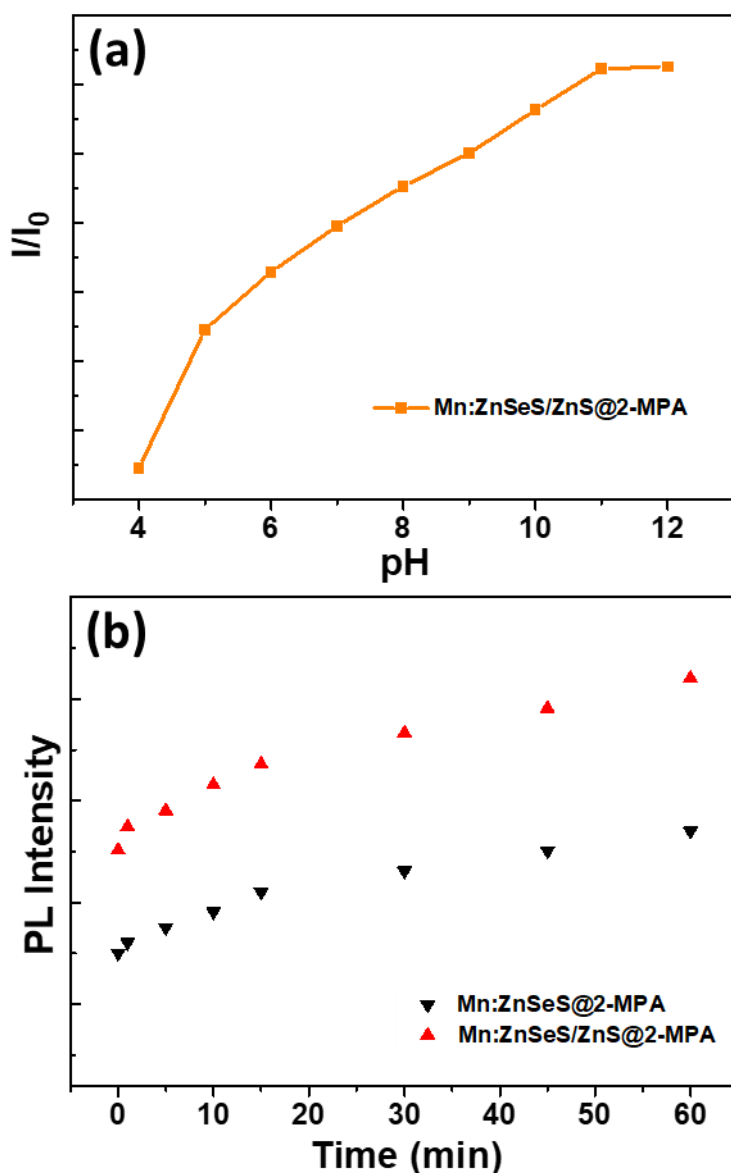


Fig. 9. (a) PL intensity of Mn:ZnSeS/ZnS@2-MPA QDs versus pH. (b) Time evolution of the PL intensity of the Mn(10):ZnSeS and Mn(10):ZnSeS/ZnS QDs under the continuous irradiation of a Hg-Xe lamp (light intensity of 50 mW/cm^2).

As prepared Mn(10):ZnSeS/ZnS QDs exhibit a relatively high hydrodynamic diameter of ca. 24 nm (Fig. 10a) with a polydispersity index (PDI) of ca. 0.22, suggesting a slight agglomeration of the dots in aqueous solution despite of their relatively high negative Zeta potential of -34 mV (Fig. 10b). When stored at room temperature in the dark or under room light, the QDs were found to be stable for at least two weeks as indicated by UV-visible absorption and PL emission spectra (Fig. S12). As can be seen, an increase of the PL intensity

for observed for the dots exposed to light, which is in good agreement with photostability studies. However, precipitates start to appear after that period of a storage. This may originate from the weak surface coverage in 2-MPA and/or from the presence of Zn-2-MPA complexes at the periphery of the dots that mask their negative charge. To increase the ligand density, Mn(10):ZnSeS/ZnS@2-MPA QDs were treated at 100°C for 3 h with aqueous solutions of GSH, NAC or 2-dimethylaminoethanethiol (DMAT) that will anchor via their thiol function to surface Zn atoms (Fig. 10c). A marked improvement of the colloidal stability was observed and no precipitate could be detected upon storage for up to 6 months. Moreover, the PL intensity of Mn(10):ZnSeS/ZnS QDs increased significantly, which confirms the reduction of surface defects by the enhanced ligand coverage (Fig. 10d and Fig. S13 for the UV-visible and PL emission spectra recorded using GSH). The asymmetric and symmetric signals of free carboxylate functions at 1580 and 1387 cm^{-1} can be observed in the FT-IR spectra of the nanocrystals treated with GSH, NAC and DMAT, which further confirms the successful ligand capping (Fig. S14). Thermogravimetric analyses (TGA) of 2-MPA and 2-MPA/GSH-capped QDs are shown in Fig. S15. For 2-MPA-capped QDs, a gradual weight loss is observed between 100 and 400°C due to the thermal decomposition of 2-MPA and of Zn^{2+} -2-MPA complexes anchored at the surface of the dots. The remaining mass is of ca. 81% and corresponds to Mn:ZnSeS/ZnS nanocrystals. The weight loss is higher for 2-MPA/GSH-capped QDs (48%) which confirms that the dots are covered by a thicker shell of ligand. Finally, the electrophoretic mobility of the native 2-MPA-capped QDs was also compared to that of QDs treated with DMAT, NAC or GSH on a cellulose acetate sheet in a borate buffer solution (pH 9.1) (Fig. 10e). The migration of QDs treated with DMAT is weak and almost similar to that of 2-MPA-capped QDs suggesting that their surface charge is neutral due to the presence of the negatively charged 2-MPA and of the positively charged DMAT ligands. Results obtained with DMAT also suggest that the 2-MPA ligand remains at the surface of the dots and is not displaced by GSH, NAC or DMAT. 2-MPA/NAC and 2-MPA/GSH-capped QDs migrate much faster than those only covered with 2-MPA indicating that their negative charge is significantly higher.

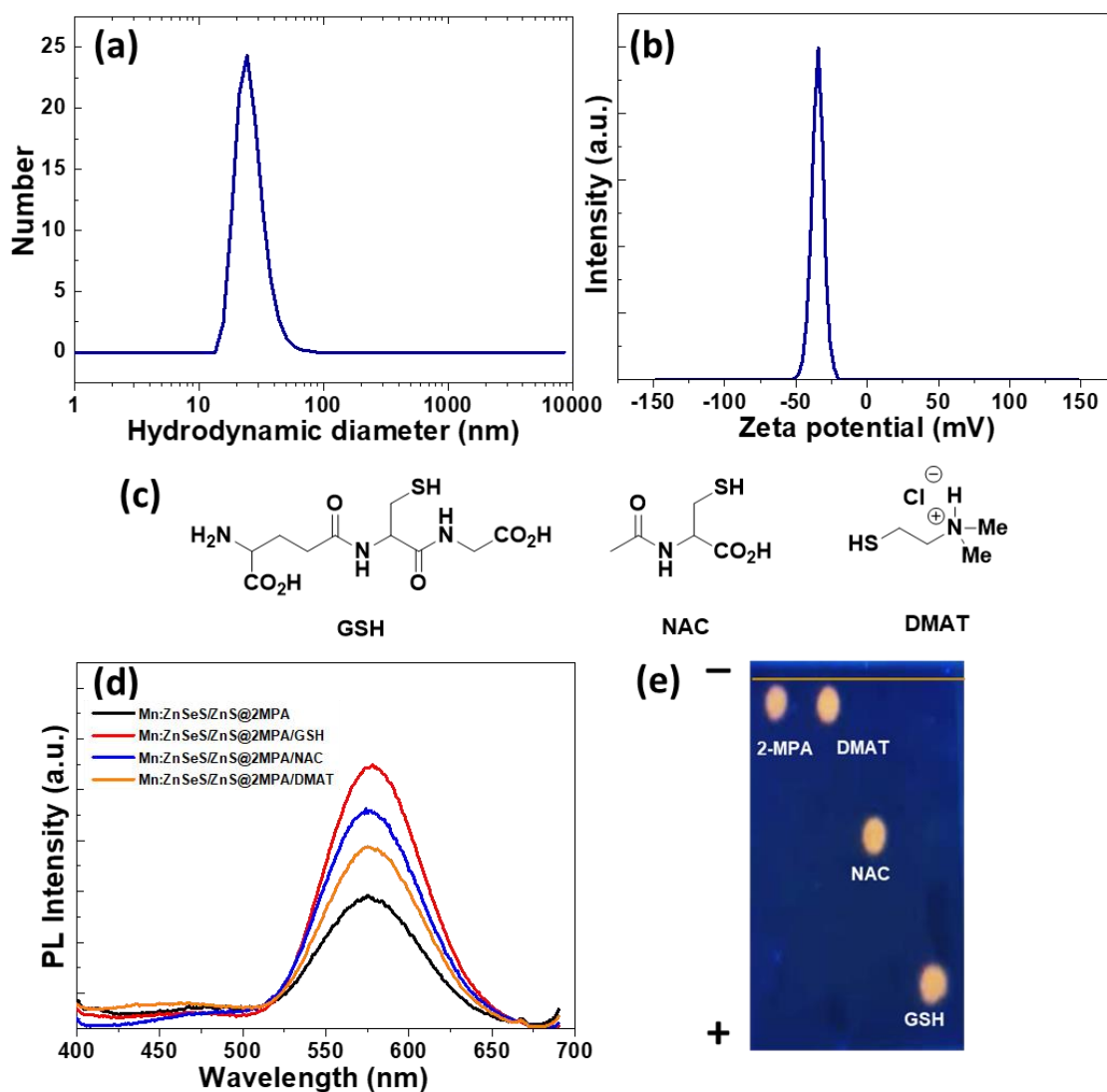


Fig. 10. (a) Hydrodynamic diameter and (b) Zeta potential of Mn(10):ZnSeS/ZnS@2-MPA QDs, (c) Chemical structures of GSH, NAC and DMAT, (d) PL emission spectra of Mn:ZnSeS/ZnS QDs after treatment with GSH, NAC or DMAT and (e) electrophoretic mobility of 2-MPA, DMAT, NAC and GSH-capped QDs on a cellulose acetate sheet.

3.5. Phase Transfer

Tuning the surface polarity of QDs is of high interest for numerous applications and depends on the ligand structure, that enables the dispersion of QDs either in polar or in nonpolar solvents. Hydrophobic QDs may be required for various applications like LED devices, functionalized surfaces and even biological applications [50,51]. To demonstrate that the hydrophilicity and the hydrophobicity of Mn:ZnSeS/ZnS QDs can be tuned, 2-MPA was

exchanged with octanethiol in a water/toluene mixture using acetone as interfacial solvent [34]. After 3 h heating at 60°C, the dots were fully transferred from the aqueous to the organic phase (Fig. 11a). Next, to repair the surface defects generated by the ligand exchange, the toluene layer containing the QDs was further refluxed at 110°C for 4 h. The replacement of 2-MPA by octanethiol was demonstrated by FT-IR by the disappearance of the symmetric carboxylate stretching at 1336 cm⁻¹ and the appearance of C-H stretching vibrations at 2923 and 2854 cm⁻¹ (Fig. S16). No significant changes were observed in the shape of UV-visible and PL emission spectra but the PL QY increased from 41% for 2-MPA-capped QDs to 46.7% for octanethiol-functionalized ones (Fig. 11b).

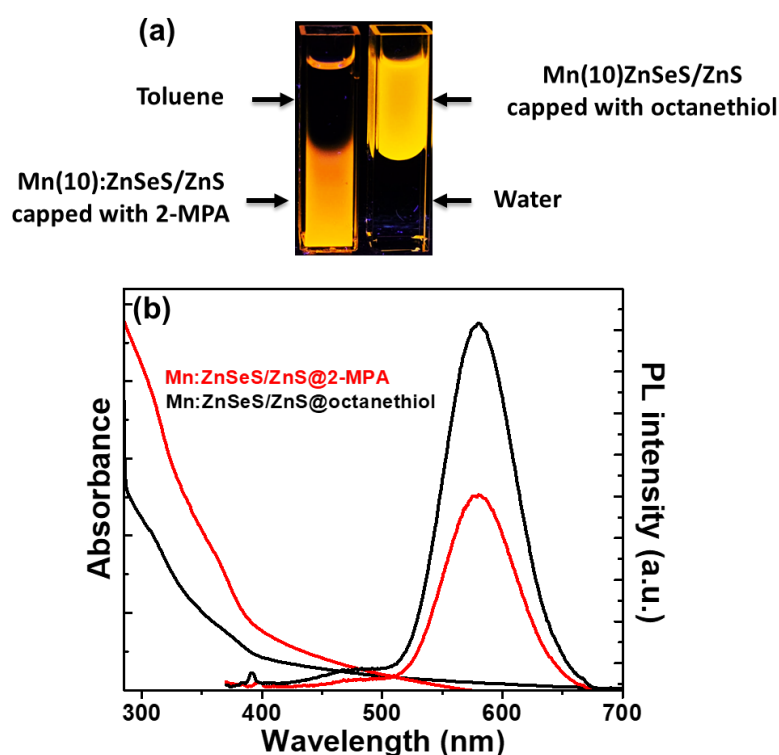


Fig. 11. (a) Digital photograph taken under UV light illumination of Mn(10):ZnSeS/ZnS QDs in a biphasic water/toluene mixture before and after the ligand exchange and (b) UV-visible absorption and PL emission spectra of Mn:ZnSeS/ZnS core/shell QDs before (red line) and after (black line) phase transfer using octanethiol.

4. Conclusion

A facile and environmentally friendly aqueous synthesis of ternary alloyed Mn:ZnSeS and core/shell Mn:ZnSeS/ZnS QDs was developed using 2-MPA as ligand. The obtained

nanocrystals are of small size (2.4 and 3.7 nm for core and core/shell QDs, respectively) and exhibit a high crystallinity. High quantum efficiencies of 22 and 41% for Mn:ZnSeS and Mn:ZnSeS/ZnS QDs, respectively, were observed and the dots are of high photostability. Mn:ZnSeS QDs exhibit also long PL lifetimes (up to 681 μ s) indicating that the emission originates from the spin forbidden $\text{Mn}^{2+} \text{}^4\text{T}_1 \rightarrow \text{}^6\text{A}_1$ transition. The optical properties of the dots are well retained after ligand exchange, further demonstrating their stability. Thus, the present study shows that Mn:ZnSeS QDs have a wide scope in various applications like biological imaging and sensing.

CRedit authorship contribution statement

Salima Mabrouk: Investigation, Data curation, Writing - original draft. **Hervé Rinnert:** Investigation, Data curation, Writing. **Lavinia Balan:** Investigation, Data curation, Writing. **Sébastien Blanchard:** Investigation, Data curation, Formal analysis. Writing. **Jordane Jasniewski:** Investigation, Formal analysis, Data curation, Writing. **Ghouthi Medjahdi:** Investigation, Data curation. **Rafik Ben Chaabane:** Supervision. **Raphaël Schneider:** Conceptualization, Methodology, Writing - review & editing, Supervision.

Declaration of competing interest

The authors declare that they have no competing financial interests or personal relationships that could have appeared to influence the work reported in this paper.

Acknowledgements

S. Mabrouk thanks the University of Monastir for financial support.

References

- [1] N.S. Karan, D.D. Sarma, R.M. Kadam, N. Pradham, Doping Transition Metal (Mn or Cu) Ions in Semiconductor Nanocrystals, *J. Phys. Chem. Lett.* 1 (2010) 2863-2866.
- [2] D.J. Norris, A.L. Efros, S.C. Erwin, Doped Nanocrystals, *Science* 319 (2008) 1776-1779.
- [3] P. Wu, X.-P. Yan, Doped quantum dots for chemo/biosensing and bioimaging, *Chem. Soc. Rev.* 42 (2013) 5489-5521.

- [4] M. Makkar, R. Viswanatha, Frontier challenges in doping quantum dots: synthesis and characterization, *RSC Adv.* 8 (2018) 22103-22112.
- [5] M. Geszke, M. Murias, L. Balan, G. Medjahdi, J. Korczynski, M. Moritz, J. Lulek, R. Schneider, Folic acid-conjugated core/shell ZnS:Mn/ZnS quantum dots as targeted probes for two photon fluorescence imaging of cancer cells, *Acta Biomaterialia* 7 (2011) 1327-1338.
- [6] A. Aboulaich, L. Balan, J. Ghanbaja, G. Medjahdi, C. Merlin, R. Schneider, Aqueous Route to Biocompatible ZnSe:Mn/ZnO Core/Shell Quantum Dots Using 1-Thioglycerol As Stabilizer, *Chem. Mater.* 2011 (2011) 3706–3713.
- [7] A. Aboulaich, M. Geszke, L. Balan, J. Ghanbaja, G. Medjahdi, R. Schneider, Water-Based Route to Colloidal Mn-Doped ZnSe and Core/Shell ZnSe/ZnS Quantum Dots, *Inorg. Chem.* 2010, 49, 10940–10948.
- [8] N. Pradham, Mn-Doped Semiconductor Nanocrystals: 25 Years and Beyond, *J. Phys. Chem. Lett.* 10 (2019) 2574-2577.
- [9] X. Yuan, J. Zheng, R. Zeng, P. Jing, W. Ji, J. Zhao, W. Yang, H. Li, Thermal stability of Mn²⁺ ion luminescence in Mn-doped core–shell quantum dots, *Nanoscale* 6 (2014) 300-307.
- [10] M. Geszke-Moritz, H. Piotrowska, M. Murias, L. Balan, M. Moritz, J. Lulek, R. Schneider, Thioglycerol-capped Mn-doped ZnS quantum dot bioconjugates as efficient two-photon fluorescent nano-probes for bioimaging, *J. Mater. Chem. B* 1 (2013) 698-706.
- [11] L. Chang, X. He, L. Chen, Y. Zhang, Mercaptophenylboronic acid-capped Mn-doped ZnS quantum dots for highly selective and sensitive fluorescence detection of glycoproteins, *Sens. Actuators B* 243 (2017) 72-77.
- [12] D.J. Norris, N. Yao, F.T. Clarnock, T.A. Kennedy, High-Quality Manganese-Doped ZnSe Nanocrystals, *Nano Lett.* 1 (2001) 3-7.
- [13] N. Pradham, D. Goorskey, J. Thessing, X. Peng, An Alternative of CdSe Nanocrystal Emitters: Pure and Tunable Impurity Emissions in ZnSe Nanocrystals, *J. Am. Chem. Soc.* 127 (2005) 17586-17587.
- [14] N. Pradham, X.G. Peng, Efficient and Color-Tunable Mn-Doped ZnSe Nanocrystal Emitters: Control of Optical Performance via Greener Synthetic Chemistry, *J. Am. Chem. Soc.* 129 (2007) 3339-3347.
- [15] B.B. Srivastava, S. Jana, N.S. Karan, S. Paria, N.R. Jana, D.D. Sarma, N. Pradham, Highly Luminescent Mn-Doped ZnS Nanocrystals: Gram-Scale Synthesis, *J. Phys. Chem. Lett.* 1 (2010) 1454-1458.

- [16] B. Yang, X. Shen, H. Zhang, Y. Cui, J. Zhang, Luminescent and Magnetic Properties in Semiconductor Nanocrystals with Radial-Position-Controlled Mn²⁺ Doping, *J. Phys. Chem. C* 117 (2013) 15829-15834.
- [17] L.-J. Zhang, X.-C. Shen, H. Liang, F.-Y. Chen, H.-J. Huang, Phosphine-free synthesis of ZnSe:Mn and ZnSe:Mn/ZnS doped quantum dots using new Se and S precursors, *New J. Chem.* 38 (2014) 448-454.
- [18] J.H. Yu, J. Kim, T. Hyeon, J. Yang, Facile synthesis of manganese (II)- doped ZnSe nanocrystals with controlled dimensionality, *J. Chem. Phys.* 151 (2019) 244701.
- [19] J. Selvaraj, A. Mahesh, V. Asokan, V. Baskaralingam, A. Dhayalan, T. Paramasivam, Phosphine-Free, Highly Emissive, Water-Soluble Mn:ZnSe/ZnS Core-Shell Nanorods: Synthesis, Characterization, and in Vitro Bioimaging of HEK293 and HeLa Cells, *ACS Appl. Nano Mater.* 1 (2018) 371-383.
- [20] C. Wang, X. Gao, Q. Ma, X. Su, Aqueous synthesis of mercaptopropionic acid capped Mn²⁺-doped ZnSe quantum dots, *J. Mater. Chem.* 19 (2009) 7016-7022.
- [21] B. Dong, L. Cao, G. Su, W. Liu, Facile Synthesis of Highly Luminescent Water-Soluble ZnSe:Mn/ZnS Core/Shell Doped Nanocrystals with Pure Dopant Emission, *J. Phys. Chem. C* 116 (2012) 12258-12264.
- [22] B.T. Luong, E. Hyeong, S. Ji, N. Kim, Green synthesis of highly UV-orange emitting ZnSe/ZnS:Mn/ZnS core/ shell/shell nanocrystals by a three-step single flask method, *RSC Adv.* 2 (2012) 12132-12135.
- [23] C. Wang, S. Xu, Y. Wang, Z. Wang, Y. Cui, Aqueous synthesis of multilayer Mn:ZnSe/Cu:ZnS quantum dots with white light emission, *J. Mater. Chem. C* 2 (2014) 660-666.
- [24] P. Reiss, M. Protière, L. Li, Core/shell semiconductor nanocrystals, *Small* 5 (2009) 154-168.
- [25] H. Qian, X. Qiu, L. Li, J. Ren, Microwave-Assisted Aqueous Synthesis: A Rapid Approach to Prepare Highly Luminescent ZnSe(S) Alloyed Quantum Dots, *J. Phys. Chem. B* 110 (2006) 9034-9040.
- [26] A. Shavel, N. Gaponik, A. Eychmuller, Efficient UV-Blue Photoluminescing Thiol-Stabilized Water-Soluble Alloyed ZnSe(S) Nanocrystals, *J. Phys. Chem. B* 108 (2004) 5905-5908.
- [27] E. Soheyli, R. Sahraei, G. Nabiyouni, F. Nazari, R. Tabaraki, B. Ghaemi, Luminescent, low-toxic and stable gradient-alloyed Fe:ZnSe(S)@ZnSe(S) core:shell quantum dots as a sensitive fluorescent sensor for lead ions, *Nanotechnology* 29 (2018) 445602.

- [28] K. Saikia, P. Deb, E. Kalita, Sensitive fluorescence response of ZnSe(S) quantum dots: an efficient fluorescence probe. *Phys. Scr.* 87 (2013) 065802.
- [29] K. Yu, A. Hrdina, J. Ouyang, D. Kingston, X. Wu, D.M. Leek, X. Liu, C. Li, Ultraviolet ZnSe_{1-x}S_x Gradient-Alloyed Nanocrystals via a Noninjection Approach, *ACS Appl. Mater. Interfaces* 4 (2012) 4302-4311.
- [30] R. Zeng, R. Shen, Y. Zhao, Z. Sun, X. Li, J. Zheng, S. Cao, B. Zou, Water-soluble, highly emissive, color-tunable and stable Cu-doped ZnSeS/ZnS core/shell nanocrystals, *CrystEngComm* 16 (2014) 3414-3423.
- [31] R. Zeng, T. Zhang, G. Dai, B. Zou, Highly Emissive, Color-Tunable, Phosphine-Free Mn:ZnSe/ZnS Core/Shell and Mn:ZnSeS Shell-Alloyed Doped Nanocrystals, *J. Phys. Chem. C* 115 (2011) 3005-3010.
- [32] J. Zimdars, J. Pilger, M. Entrup, D. Deiting, A.H. Schäfer, M. Bredol, A facile synthesis of alloyed Mn-doped ZnSeS nanoparticles using a modified selenium/sulfur precursor in a one-pot approach, *New J. Chem.* 40 (2016) 8465-8470.
- [33] B. Ke, X. Bai, R. Wang, Y. Shen, C. Cai, K. Bai, R. Zeng, B. Zou, Z. Chen, Alkylthiol-enabled Se powder dissolving for phosphine-free synthesis of highly emissive, large-sized and spherical Mn-doped ZnSeS nanocrystals, *RSC Adv.* 7 (2017) 44867-44873.
- [34] H. Nishimura, Y. Lin, M. Hizume, T. Taniguchi, N. Shigekawa, T. Takagi, S. Sobue, S. Kawai, E. Okuno, D. Kim, Synthesis of Mn-Doped ZnSe-ZnS Alloy Quantum Dots by a Hydrothermal Method, *Chem. Lett.* 48 (2019) 1081-1083.
- [35] S. Ithurria, P. Guyot-Sionnest, B. Mahler, B. Dubertret, Mn²⁺ as a radial pressure gauge in colloidal core/shell nanocrystals, *Phys. Rev. Lett.* 99 (2007) 265501.
- [36] J.M. Tsay, M. Pflughoefft, L.A. Bentolila, S. Weiss, Hybrid Approach to the Synthesis of Highly Luminescent CdTe/ZnS and CdHgTe/ZnS Nanocrystals, *J. Am. Chem. Soc.* 126 (2004) 1926-1927.
- [37] C. Ye, X. Fang, G. Li, L. Zhang, Origin of the green photoluminescence from zinc sulfide nanobelts, *Appl. Phys. Lett.* 85 (2004) 3035-3037.
- [38] S. Wageh, Z. Su Ling, X. Xu-Rong, Growth and optical properties of colloidal ZnS nanoparticles, *J. Cryst. Growth* 255 (2003) 332-337.
- [39] C. Gan, Y. Zhang, D. Battaglia, X. Peng, M. Xiao, Fluorescence lifetime of Mn-doped ZnSe quantum dots with size dependence, *Appl. Phys. Lett.* 2008, 92, 241111.
- [40] H.Y. Acar, R. Kas, E. Yurtsever, C. Ozen, I. Lieberwirth, Emergence of 2MPA as an effective coating for highly stable and luminescent quantum dots, *J. Phys. Chem. C* 113 (2009) 10005-10012.

- [41] D. Vasudevan, A. Trinchi, S.G. Hardin, I.S. Cole, Fluorescent heavy metal cation sensing with water dispersible 2MPA capped CdSe/ZnS quantum dots, *J. Lumin.* 166 (2015) 88-92.
- [42] N. Mahapatra, A. Mandal, S. Panja, M. Halder, Emergence of the selective ultra-sensing of Ag(I): Thiolactic acid as efficient capping agent for cadmium chalcogenide quantum dots in modulating photoluminescence and metal reception, *Sens. Actuators B* 240 (2017) 543-552.
- [43] T. Rajh, D.M. Tiede, M.C. Thurnauer, Surface modification of TiO₂ nanoparticles with bidentate ligands studied by EPR spectroscopy, *J. Non-Cryst. Solids* 205-207 (1996) 815-820.
- [44] M. Aguilar, S. Alegret, E. Casassas, Complex formation between Cd(II) and 2-mercaptopropionic acid in 3.0 M NaClO₄ at 25°C, *J. Inorg. Nucl. Chem.* 39 (1977) 733-737.
- [45] A.D. Patel, J.D. Joshi, Synthesis, characterization and antimicrobial activities of nickel (II), zinc(II) and cadmium(II) chelates with 2,2'-bipyridylamine and thio acids, *Synth. React. Inorg. Met. -Org. Chem.* 25 (1995) 991-1010.
- [46] B.J. Park, W.B. Im, W.J. Chung, H.S. Seo, J.T. Ahn, Internal pressure effect on cathodoluminescence enhancement of ZnS:Mn²⁺ synthesized by a sealed vessel, *J. Mater. Res.* 22 (2007) 2838-2844.
- [47] L. Zu, A.W. Wills, T.A. Kennedy, E.R. Glaser, D.J. Norris, Effect of Different Manganese Precursors on the Doping Efficiency in ZnSe Nanocrystals, *J. Phys. Chem. C* 114 (2010) 21969-21975.
- [48] J.J. Wang, Y.Q. Wang, F.F. Cao, Y.G. Guo, L.J. Wan, Synthesis of Monodispersed Wurtzite Structure CuInSe₂ Nanocrystals and Their Application in High-Performance Organic-Inorganic Hybrid Photodetectors, *J. Am. Chem. Soc.* 132 (2010) 12218.
- [49] K. Qi, R. Selvaraj, U. Jeong, S.M.Z. Al-Kindy, M. Sillanpaa, Y. Kim, C.-w. Tai, Hierarchical-like multipod γ -MnS microcrystals: Solvothermal synthesis, characterization and growth mechanism, *RSC Adv.* 5 (2015) 9618-9620.
- [50] F. Aldeek, C. Mustin, L. Balan, T. Roques-Carmes, M.-P. Fontaine-Aupart, R. Schneider, Surface-engineered quantum dots for the labeling of hydrophobic microdomains in bacterial biofilms, *Biomaterials* 32 (2011) 5459-5470.
- [51] K.C. Elbert, D. Jishkariani, Y. Wu, J.D. Lee, B. Donnio, C.B. Murray, Design, self-assembly, and switchable wettability in hydrophobic, hydrophilic, and Janus dendritic ligand-gold hybrid materials, *Chem. Mater.* 29 (2017) 8737-8746.